Journal Pre-proofs

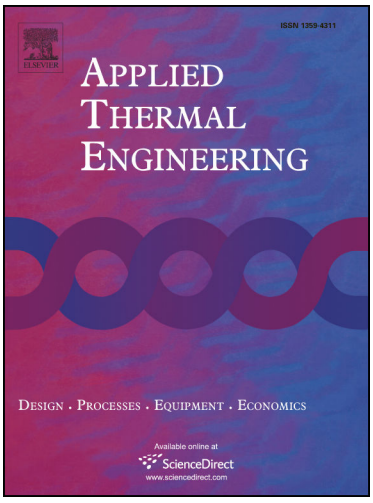

A novel refrigerant-direct radiant cooling system: numerical simulation-based evaluation

Tingting Jiang, Shijun You, Zhangxiang Wu, Huan Zhang, Yaran Wang, Shen Wei

PII: S1359-4311(21)00876-0
DOI: https://doi.org/10.1016/j.applthermaleng.2021.117442
Reference: ATE 117442

To appear in: *Applied Thermal Engineering*

Received Date: 5 March 2021
Revised Date: 25 July 2021
Accepted Date: 6 August 2021

Please cite this article as: T. Jiang, S. You, Z. Wu, H. Zhang, Y. Wang, S. Wei, A novel refrigerant-direct radiant cooling system: numerical simulation-based evaluation, *Applied Thermal Engineering* (2021), doi: https://doi.org/10.1016/j.applthermaleng.2021.117442

A novel refrigerant-direct radiant cooling system: numerical simulation-based evaluation

Tingting Jiang [a], Shijun You [a, b], Zhangxiang Wu [a], Huan Zhang [a, b], Yaran Wang [a, b,*], Shen Wei [c]

[a] School of Environmental Science and Engineering, Tianjin University, Haihe Education Area, Jinnan District, Tianjin 300350, PR China

[b] Key Laboratory of Efficient Utilization of Low and Medium Grade Energy (Tianjin University), Ministry of Education of China, Tianjin 300350, PR China.

[c] The Bartlett School of Construction and Project Management, University College London (UCL), 1-19 Torrington Place, London WC1E 7HB, United Kingdom.

Abstract

Split air-conditioners have deficiency in thermal comfort due to its draught sensation and fan noise. The existing radiant cooling systems adopt chilled water as circulating medium, leading to low energy efficiency because of the requirement of

* Corresponding author. Tel.: +8602227892626; fax: +8602227892626.

E-mail addresses: yaran_wang@tju.edu.cn

secondary heat exchange. To address these problems, a novel refrigerant-direct radiant cooling (RDRC) system is proposed. Experiments are conducted in a climate chamber to evaluate the thermal performance of this system. Results show that the RDRC terminal surface temperature is distributed homogenously and this system has excellent stability. The mathematical and economic models of this terminal are established and the mathematical model is validated with the measured data. The effects of different structural parameters on thermal and economic performances of the RDRC system are investigated, and then this terminal is optimized by orthogonal design method. The cooling capacity for per exterior area is considered as objective function and the initial cost less than 121.1 $ is taken as constraint condition. Results indicate that the fin height of 40.0 mm, the copper pipe diameter of 6.0 mm, the copper pipe spacing of 40.0 mm and the aspect ratio of 0.88 are recommended.

Keywords: refrigerant-direct radiant cooling system; mathematical and economic models; thermal and economic performances; optimal structure

Nomenclature

A	area (m^2)	**Greek symbols**	
B	Chisholm parameter	λ	thermal conductivity ($W\cdot m^{-1}\cdot K^{-1}$)
Bo	boiling number	δ	thickness (mm)
b_w	simplified coefficient	ε	emissivity

C	constant of Lockhart and Martinelli parameter	ρ	density (kg· m^{-3})
c_p	specific heat (J· kg^{-1}· K^{-1})	σ	Stefan-Boltzmann constant, (5.67×10^{-8} W· m^{-2}· K^{-4})
D	diameter (mm)	μ	dynamic viscosity (Pa· s)
E	enhancement factor	α	volume expansion coefficient (1· K^{-1})
fr	friction factor	v	kinematic viscosity (m^2· s)
G	refrigerant mass flow rate (kg· s^{-1})	φ	relative humidity (%)
Gr	Grashof number	ϕ	multiplier factor
g_a	acceleration of gravity (m· s^{-2})	η	efficiency (%)
H	height (mm)	***Subscripts***	
h	convective heat transfer coefficient (W· m^{-2}· K^{-1})	co	copper pipe
h_D	conversion heat release coefficient (W· m^{-2}· K^{-1})	coi	inner surface of copper pipe
I	enthalpy (J· kg^{-1})	coo	outer surface of copper pipe
J	effective radiation (W· m^{-2})	cond	conduction
L	length (m)	conv	convection
M	molecular weight	conde	condensation
m	mass velocity of refrigerant (kg· m^{-2}· s^{-1})	e	evaporate
Nu	Nusselt number	ea	exterior area
n	number of sections	fe	fin-end
Pr	Prandtl number	g	gas
p	pressure (Pa)	i	node i
p_c	critical pressure (Pa)	inl	inlet
Q	cooling capacity (W)	l	liquid
q	heat flux (W· m^{-2})	le	labor expense
Re	Reynolds number	n	indoor air
R	thermal resistance (m^2· K· W^{-1})	out	outlet
R'	range	pb	pool boiling
S	suppression factor	r	refrigerant
r	rate (kg· s^{-1})	rad	radiation
t	temperature (^{o}C)	se	connection segment

t_m	mean surface temperature (°C)	sim	simulated
v	superficial velocity (m· s^{-1})	sp	spacing
w	width (mm)	st	steel panel channel with copper pipe
X	angle coefficient	stk	steel panel channel with water
X_{tt}	Martinelli parameter	t	total
x	vapor quality	wa	wa
z	shape parameter of fins	wf	water film
Δh_{lv}	latent heat of vaporization (J· kg^{-1})	**Abbreviations**	
Δl	control volume length (m)	RDRC	refrigerant-direct radiant cooling
Δp	pressure drop (Pa)	*IC*	initial cost
Δt	temperature difference (°C)		

1. Introduction

With the improvement of living standards, the requirements of indoor comfortable environment are gradually increasing, while the building energy consumption increases as well [1]. Traditional split air-conditioners depend on forced convection only, which have the defects of poor thermal comfort and low energy efficiency [2]. It is essential to develop new techniques with the merits of improving indoor thermal comfort and degrading energy consumption.

Radiant cooling systems have been drawn much attention in recent years, which can achieve good thermal comfort and high energy efficiency [3]. Catalina et al. [4] investigated the performance of a radiant cooling ceiling through numerical simulation, and the results showed that this system could achieve small vertical temperature

gradient and low air velocity, which were less than 1 $^{o}C\cdot m^{-1}$ and 0.1 $m\cdot s^{-1}$. Kitagawa et al. [5] evaluated the thermal comfort of a radiant cooling system based on the thermal sensation vote, illustrating that the most comfortable sensation vote was around -0.5 rather than neutral. Niu et al. [6] analyzed the annual energy consumption of a hybrid chilled-ceiling system and justified that this system could reduce 44% primary energy due to the improvement of evaporating temperature. A field study of a radiant air-conditioning system was carried out by Peng et al. [7] in south-central China, with results showing that this system was able to save 26.4% energy in comparison with split air-conditioners.

Researchers also have investigated the heat transfer characteristics and design optimization of radiant cooling systems to obtain better thermal performance. Xia et al. [8] launched a theoretical research of the metal ceiling radiant cooling panel and suggested that the flow rate, fluid inlet temperature and architecture materials exert significant roles in evaluating the heat transfer performance of this system. Li et al. [9] presented a new heat transfer formula of the radiant floor system based on the simulation model, with results showing that the floor surface temperature distribution and the thermal performance of this system could be predicted precisely. Tian et al. [10] developed a heat transfer model to explore the cooling performance of ceiling radiant

cooling panels. The results confirmed that the cooling capacity of this system was 17.1% higher than the manufacture's data under the condition of the characteristic temperature difference with 8 ^{o}C. A dynamic model of the thermoelectric radiant ceiling panel system was established by Luo et al. [11], justifying its contribution to predicting heat transfer performance, structure design and operating control. Shen et al. [12] developed a simplified representation method to predict thermal characteristics and provided the optimal design configurations for the thermoelectric radiant air-conditioning system, indicating that the thickness of radiant panels with 4 mm and the number of thermoelectric modules with 16 m^2 should be adopted. Su et al. [13] launched a simulation model to clarify the heat transfer mechanism of the radiant ceiling panel system and then optimized its structural parameters. The results showed that the suitable design of radiant ceiling panels was the thickness with 4.0-5.0 mm and the copper pipes with small diameter. Mosa et al. [14] used a numerical simulation method to explore the impact of flow channel configurations on overall performance of the radiant cooling panel, and the results confirmed that the dendritic structure could improve the cooling capacity and reduce pump power. The advisable configuration and spacing of the thermoelectric modules (TEMs) for radiant cooling system were conducted by Lim et.al. [15], and suggested that the best choice of this system was the TEMs with triangular

architecture and the spacing with 0.28 m.

However, when the radiant cooling systems are used to provide space cooling, the moisture condensation phenomenon on the radiant terminal surface cannot be ignored [16]. The main reason is that the radiant terminal surface temperature is lower than the dew point temperature of indoor air [17]. To tackle this issue, Ning et al. [18] developed a numerical model to optimize the structure of the cooling radiant ceiling panel with thin air layer, with the results showing that an air layer was competent to reduce temperature difference of panel surface, avoid condensation and improve the cooling capacity. Xu et al. [19] centered on the thermal performance of an air-carrying energy radiation air-conditioning system through CFD simulation, and proved that this system could prevent condensation and improve the heat transfer capacity in comparison with traditional radiant plate systems. Hernández et al. [20] conducted an experimental investigation of the new terminal unit integrating a radiant cooling floor with an underfloor air distribution system. The results indicated that this system had the potential of degrading the condensation risk, increasing the cooling capacity and reducing the response time of space load change. In addition, many scholars have concentrated on the radiant cooling systems combined with additional dehumidification systems to prevent condensation. Zhang et al. [21] proposed a new method to mitigate

condensation risk of the hybrid cooling system, which integrated the chilled ceiling with independent air dehumidification systems, and suggested that the process of dehumidification and ventilation should be implemented in advance until this system worked stably. Sui et al. [22] investigated the performance of a radiant chilled ceiling system coupled with an air handing unit, and the results showed that this system was able to prevent dew condensation effectively in hot and humid climate. A simulation method was established by Seo et al. [23] to confirm the possibility of a radiant floor cooling system associated with dehumidified ventilation in Korea, justifying its contribution to avoiding the risk of dew condensation.

Nevertheless, these additional devices will increase the complexity of radiant cooling systems and initial cost. Besides, the existing radiant cooling systems generally use chilled water as working fluid with low energy efficiency. To tackle these issues, a novel refrigerant-direct radiant cooling (RDRC) system is proposed in this paper. This system adopts refrigerant as circulating medium to avoid secondary heat exchange. Additionally, there is no need of independent dehumidification systems since it allows dew condensation behavior on the RDRC terminal surface to mitigate indoor moisture content, which can reduce the system complexity and initial cost. Therefore, the RDRC system is suitable for application in residential buildings due to its simple structure. In

order to improve the thermal and economic performances of this system, exploring the optimal structure of the RDRC terminal is a pivotal task. In this study, the mathematical and economic models of the RDRC terminal are established, and the mathematical model is validated with the experimental data. Then the impacts of the fin height, copper pipe diameter, copper pipe spacing as well as aspect ratio on thermal and economic performances of this system are investigated. Finally, the influencing degree of these factors and the optimal structure of this terminal are obtained.

2. Mathematical model

2.1 Physical model

Fig. 1 shows the schematic of the RDRC terminal, which consists of steel panels, copper pipes, water, fins and condensation collection plate. The flow passages are made of serpentine copper pipes with four parallel paths and are arranged at regular intervals in the steel panels. The copper pipes are filled with R410a refrigerant for its environmental friendliness. The vertical fins are attached to the steel panels to enhance heat transfer between the RDRC terminal and indoor environment. Water as the cold-storage medium is sandwiched between copper pipes and steel panels. The weight of water is 10.9 kg. The water-injection hole and air-releasing hole are placed at the top

of the RDRC terminal. The condensation collection plate is installed at the bottom to collect condensation water and then discharge it to outside through drain pipes. Fig. 2 depicts the heat transfer resistance network between the RDRC terminal and indoor environment. During the test, the indoor air and interior surface of walls exchange heat with the steel panels and fins through radiation and natural convection, and then the heat is delivered to the water via heat conduction. Subsequently, the water transfers heat to the outer surface of copper pipes by heat conduction, and then to the inner surface of copper pipes by heat conduction as well. Finally, the heat taken from the inner surface of copper pipes is transferred to the refrigerant through heat convection.

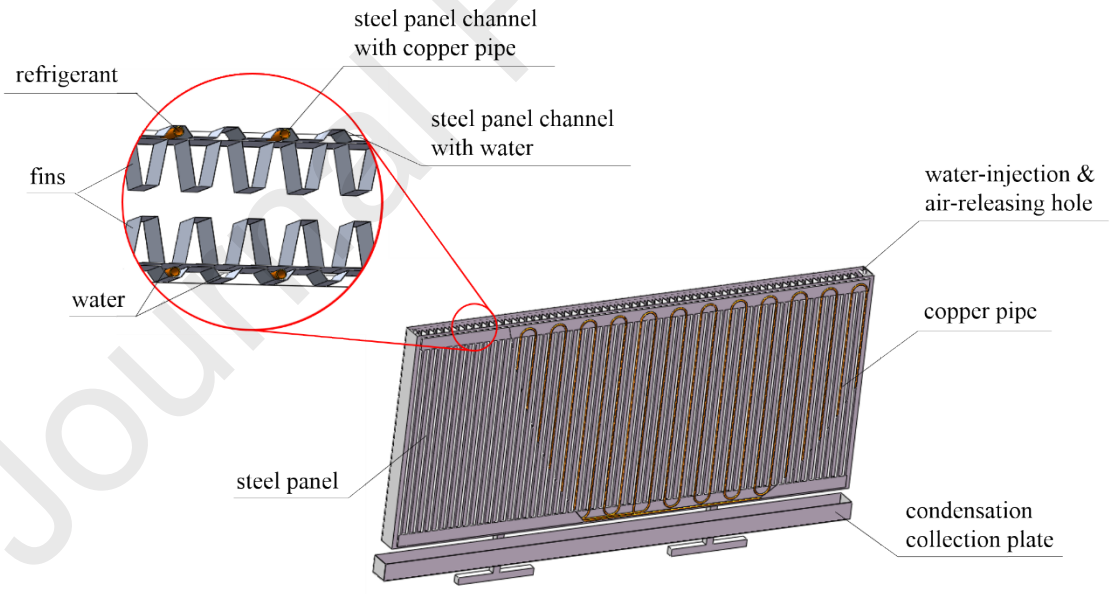

Fig. 1. The schematic of the RDRC terminal.

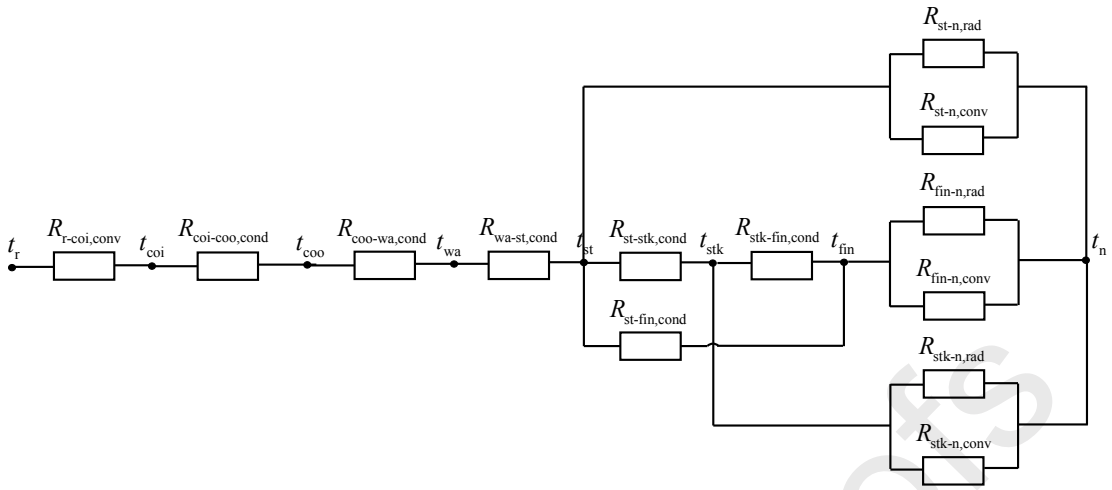

Fig. 2. The heat transfer resistance network between the RDRC terminal and indoor environment.

To simplify the mathematical model of the RDRT terminal, the following assumptions are considered as: (1) the cooling performance is investigated when the RDRT terminal reaches thermal equilibrium, therefore, a one-dimensional and steady-state model is adopted; (2) the vertical channel of the RDRT terminal is made up of many concentric cylinders; (3) the water between copper pipes and steel panels is regarded as static; (4) the heat conduction in axial-direction of the refrigerant, copper pipes, water and steel panels is neglected; (5) indoor air temperature and wall temperature are evenly distributed.

2.2 Heat transfer model of the RDRC terminal

2.2.1 Convective heat transfer of the refrigerant

The cooling energies of the refrigerant in two-phase and gas-phase states, $Q_{\text{two-phase}}$ and $Q_{\text{gas-phase}}$ are calculated by Eq. (1) and Eq. (2):

$$Q_{\text{two-phase}} = G \cdot (I_{\text{r-out}} - I_{\text{r-inl}}) \qquad (0 < x_i < 1) \tag{1}$$

$$Q_{\text{gas-phase}} = c_{pg} \cdot G \cdot (t_{\text{r-out}} - t_{\text{r-inl}}) \qquad (x_i = 1) \tag{2}$$

$$Q_{\text{t}} = Q_{\text{two-phase}} + Q_{\text{gas-phase}} \tag{3}$$

$$I_{\text{r},i} = x_i \cdot I_{\text{rl},i} + (1 - x_i) \cdot I_{\text{rg},i} \tag{4}$$

where G is the refrigerant mass flow rate; $I_{\text{r-inl}}$ and $I_{\text{r-out}}$ are the inlet and outlet enthalpies of the refrigerant; c_{pg} is the specific heat of the refrigerant in gas state; $t_{\text{r-inl}}$ and $t_{\text{r-out}}$ are the inlet and outlet temperatures of the refrigerant; Q_{t} is the total cooling capacity; I_{rl} and I_{rg} are the enthalpies of the refrigerant in liquid and gas states; x is the vapor quality of the refrigerant, $0 < x < 1$ represents the refrigerant in two-phase state and $x = 1$ represents the refrigerant in gas state.

2.2.2 Heat transfer between refrigerant and copper pipe

The heat transfer between refrigerant and copper pipe is composed of two sections:

(a) heat transfer between refrigerant and inner surface of copper pipe, and (b) heat transfer between inner surface and outer surface of copper pipe.

As the flow boiling heat transfer is composed of nucleation boiling and convection evaporation, the heat transfer coefficients of the refrigerant in two-phase and gas-phase states, $h_{\text{r-coi}}$ are formulated as [24]:

$$h_{\text{r-coi}} = Eh_{\text{l}} + Sh_{\text{pb}} \qquad (0 < x_i < 1) \tag{5}$$

$$h_{\text{r-coi}} = 0.023 \cdot Re_{\text{g}}^{0.8} Pr_{\text{g}}^{0.4} \frac{\lambda_{\text{g}}}{D_{\text{r}}} \qquad (x_i = 1) \tag{6}$$

where E is the enhancement factor; h_{l} is the convective heat transfer coefficient of the refrigerant in liquid state; S is the suppression factor; h_{pb} is the pool boiling heat transfer coefficient of the refrigerant; Re_{g} and Pr_{g} are the Reynolds number and Prandtl number of the refrigerant in gas state; λ_{g} is the thermal conductivity of the refrigerant in gas state; D_{r} is the inner diameter of the copper pipe. The detailed expressions of these parameters are given in Appendix A.

The pressure drop models of the refrigerant in two-phase and gas-phase states, $\Delta p_{\text{two-phase}}$ and $\Delta p_{\text{gas-phase}}$ can be formulated as [25]:

$$\Delta p_{\text{two-phase}} = \phi_{\text{l}}^2 \Delta p_{\text{l}} \qquad (0 < x_i < 1) \tag{7}$$

$$\Delta p_{\text{gas-phase}} = \phi_{\text{g}}^2 \Delta p_{\text{g}} \qquad (x_i = 1) \tag{8}$$

where ϕ_l and ϕ_g are the multiplier factors of the refrigerant in liquid and gas states, which are calculated using Eq. (9) and Eq. (10); Δp_l and Δp_g are the pressure drops of the refrigerant in liquid and gas states, using Eq. (12) and Eq. (13):

$$\phi_l^2 = 1 + \frac{C}{X_{tt}} + \frac{1}{X_{tt}^2} + B \qquad (0 < x_i < 1) \tag{9}$$

$$\phi_g^2 = 1 + C \cdot X_{tt} + X_{tt}^2 \qquad (x_i = 1) \tag{10}$$

$$B = 36.371\left[(\frac{g_a \cdot D_r}{v^2})(1 - \frac{\rho_g}{\rho_l}) \right]^{1.278} 0.995^{\left[x - (\frac{\rho_l}{\rho_g})^{-0.01} (\frac{\mu_l}{\mu_g})^{0.77} (\frac{\sqrt{g_a \cdot D_r}}{v})^{0.41} \right]^2} \tag{11}$$

$$\Delta p_l = 4 fr_l (\frac{\Delta l}{D_r}) m^2 (1-x)^2 (\frac{1}{2\rho_l}) \qquad (0 < x_i < 1) \tag{12}$$

$$\Delta p_g = 4 fr_g (\frac{\Delta l}{D_r}) m^2 \cdot x^2 (\frac{1}{2\rho_l}) \qquad (x_i = 1) \tag{13}$$

$$fr_l = \frac{0.079}{Re_l^{0.25}}, \quad fr_g = \frac{0.079}{Re_g^{0.25}} \tag{14}$$

where C is the constant of Lockhart and Martinelli parameter and B is the Chisholm parameter, which are both proposed by Chisholm [26]. g_a is the acceleration of gravity; v is the superficial velocity of the RDRC terminal surface; fr_l and fr_g are the friction factors of the refrigerant in liquid and gas states; m is the mass velocity of the refrigerant.

Therefore, the cooling energy between refrigerant and inner surface of copper pipe, $Q_{r\text{-}coi}$ is given by:

$$Q_{r\text{-}coi} = \pi D_r \cdot \Delta l \cdot h_{r\text{-}coi} \cdot (t_r - t_{coi}) \tag{15}$$

where Δl is the length of control volume; t_{coi} is the temperature of the inner surface of

copper pipe; t_r is the temperature of the refrigerant.

The inner surface of copper pipe exchanges heat with the outer surface of copper pipe via heat conduction, and the cooling energy can be determined as:

$$Q_{\text{coi-coo}} = \frac{t_{\text{coi}} - t_{\text{coo}}}{\frac{1}{2\pi\lambda_{\text{coi}}} \ln \frac{D_{\text{coo}}}{D_{\text{r}}}} \tag{16}$$

where t_{coo} is the temperature of the outer surface of copper pipe; λ_{coi} is the thermal conductivity of the copper pipe; D_{coo} is the outer diameter of the copper pipe.

2.2.3 Heat transfer between copper pipe and steel panel

The heat transfer between copper pipe and steel panel consists of three components: (a) heat transfer between outer surface of copper pipe and water, (b) heat transfer between water and steel panel channel with copper pipe, and (c) heat transfer between steel panel channel with copper pipe and steel panel channel with water. All heat transfer mechanisms depend on heat conduction.

The cooling energy between outer surface of copper pipe and water, $Q_{\text{coo-wa}}$ is defined as:

$$Q_{\text{coo-wa}} = \frac{t_{\text{coo}} - t_{\text{wa}}}{\frac{1}{2\pi\lambda_{\text{wa}}} \ln \frac{D_{\text{wa}}}{D_{\text{coo}}}} \tag{17}$$

where t_{wa} is the temperature of the water; λ_{wa} is the thermal conductivity of the water; D_{wa} is the diameter of the water.

The cooling energy between water and steel panel channel with copper pipe, $Q_{\text{wa-st}}$ is written as:

$$Q_{\text{wa-st}} = \frac{t_{\text{wa}} - t_{\text{st}}}{\frac{1}{2\pi\lambda_{\text{st}}} \ln \frac{D_{\text{st}}}{D_{\text{wa}}}} \tag{18}$$

where t_{st} is the temperature of the steel panel channel with copper pipe; λ_{st} is the thermal conductivity of the steel panel; D_{st} is the diameter of the steel panel channel with copper pipe.

The cooling energy between steel panel channel with copper pipe and steel panel channel with water, $Q_{\text{st-stk}}$ is described as:

$$Q_{\text{st-stk}} = \lambda_{\text{st}} \cdot \frac{t_{\text{st}} - t_{\text{stk}}}{\delta_{\text{se}}} \cdot A \tag{19}$$

where t_{stk} is the temperature of the steel panel channel with water; δ_{se} and A are the thickness and cross-sectional area of the connection segment.

2.2.4 Heat transfer between steel panel and indoor space

The heat transfer between steel panel and indoor space is composed of five sections: (a) radiative heat transfer between steel panel and indoor space, (b) radiative heat transfer between fin and indoor space, (c) convective heat transfer between steel panel and indoor space, (d) convective heat transfer between fin and indoor space, and (e) convective heat transfer between fin-end and indoor space.

The radiative cooling energies between steel panel and indoor space, $Q_{\text{rad-st}}$ and $Q_{\text{rad-stk}}$ are given by [27]:

$$\begin{cases} J_{\text{st}} = \varepsilon\sigma t_{\text{st}}^4 + (1-\varepsilon)\sum_{i=1}^{n} J_{\text{st}} X_{i,j} \\ Q_{\text{rad-st}} = \dfrac{A\varepsilon}{1-\varepsilon}(\sigma t_{\text{st}}^4 - J_{\text{st}}) \end{cases} \quad i = 1, 2, \cdots n \tag{20}$$

$$\begin{cases} J_{\text{stk}} = \varepsilon\sigma t_{\text{stk}}^4 + (1-\varepsilon)\sum_{i=1}^{n} J_{\text{stk}} X_{i,j} \\ Q_{\text{rad-stk}} = \dfrac{A\varepsilon}{1-\varepsilon}(\sigma t_{\text{stk}}^4 - J_{\text{stk}}) \end{cases} \quad i = 1, 2, \cdots n \tag{21}$$

where J_{st} and J_{stk} represent the effective radiations of the steel panel channel with copper pipe and the steel panel channel with water; ε is the emissivity; σ is the Stefan-Boltzmann constant; $X_{i,j}$ is the angle coefficient; $Q_{\text{rad-st}}$ is the radiative cooling energy between steel panel channel with copper pipe and indoor space; $Q_{\text{rad-stk}}$ is the radiative cooling energy between steel panel channel with water and indoor space.

The radiative cooling energy between fin and indoor space, $Q_{\text{rad-fin}}$ is defined as [27]:

$$\begin{cases} J_{\text{fin}} = \varepsilon\sigma t_{\text{fin}}^4 + (1-\varepsilon)\sum_{i=1}^{n} J_{\text{fin}} X_{i,j} \\ Q_{\text{rad-fin}} = \dfrac{A\varepsilon}{1-\varepsilon}(\sigma t_{\text{fin}}^4 - J_{\text{fin}}) \end{cases} \quad i = 1, 2, \cdots n \tag{22}$$

where J_{fin} is the effective radiation of the fin; t_{fin} is the temperature of the fin.

The convective cooling energies between steel panel and indoor space, $Q_{\text{conv-st}}$ and $Q_{\text{conv-stk}}$ can be expressed as:

$$Q_{\text{conv-st}} = \frac{h_{\text{air}}}{c_{p-\text{air}}}(I_{\text{air}} - I_{\text{st}}) \cdot (\pi D_{\text{st}} \Delta l + \delta_{\text{se}} \cdot \Delta l \cdot 2) \tag{23}$$

$$Q_{\text{conv-stk}} = \frac{h_{\text{air}}}{c_{p-\text{air}}}(I_{\text{air}} - I_{\text{stk}}) \cdot (\pi D_{\text{st}} \Delta l + \delta_{\text{se}} \cdot \Delta l \cdot 2) \tag{24}$$

where h_{air} is the natural convective heat transfer coefficient [28] and its expression is depicted in Appendix B; $c_{p\text{-air}}$ is the specific heat of air; I_{air} is the enthalpy of air; I_{st} is the enthalpy of the saturated air boundary layer on steel panel channel with copper pipe; I_{stk} is the enthalpy of the saturated air boundary layer on steel panel channel with water.

The convective cooling energy between fin and indoor space, $Q_{\text{conv-fin}}$ is formulated as:

$$Q_{\text{conv-fin}} = \frac{2h_D(I_{\text{air}} - I_{\text{fin}})}{b_w} \cdot \frac{th(z\Delta l)}{z} \cdot 2 \tag{25}$$

$$\frac{1}{h_D} = \frac{\delta_{\text{wf}}}{\lambda_{\text{wf}}} + \frac{c_{p-\text{air}}}{b_w h_{\text{air}}} \tag{26}$$

$$z = \sqrt{\frac{h_D}{\lambda_{\text{fin}} \cdot \delta_{\text{fin}}}} \tag{27}$$

where h_D is the conversion heat release coefficient of the air side on fin surface; I_{fin} is the enthalpy of the saturated air boundary layer on fin surface; b_w is the simplified coefficient of air enthalpy; z is the shape parameter of the fin; δ_{wf} is the thickness of the water film; λ_{wf} is the thermal conductivity of the water film; λ_{fin} is the thermal conductivity of the fin; δ_{fin} is the thickness of the fin.

The convective cooling energy between fin-end and indoor space, $Q_{\text{conv-fe}}$ can be written as:

$$Q_{\text{conv-fe}} = \frac{h_{\text{air}}}{c_{p-\text{air}}}(I_{\text{air}} - I_{\text{fe}}) \cdot w_{\text{fe}} \cdot \Delta l \cdot 2 \tag{28}$$

where I_{fe} is the enthalpy of the saturated air boundary layer on fin-end surface; w_{fe} is the width of the fin-end.

2.3 Governing equations

Fig. 2 depicts the control volumes along the refrigerant flow direction, which are divided into n sections and the length of each control volume is Δl. Based on the finite volume method, the governing equations for i node are established, as follows:

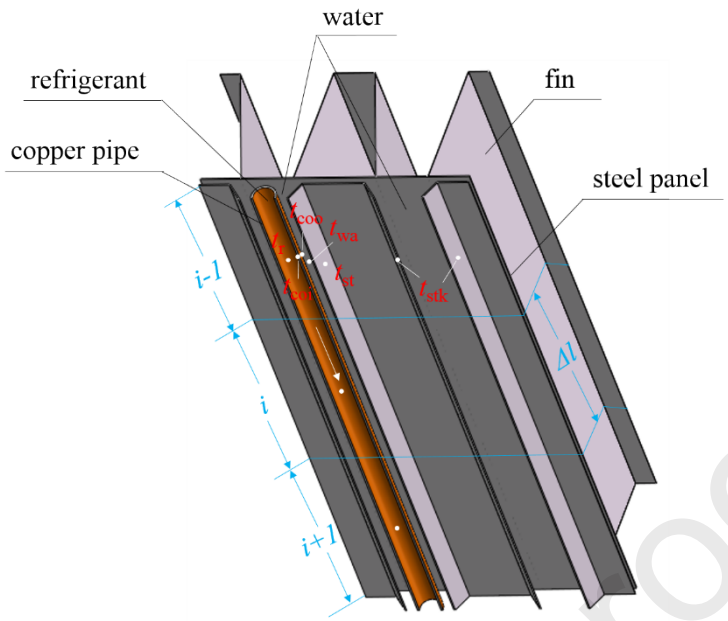

Fig. 2. Sketch of control volumes of the RDRC terminal.

For the refrigerant:

$$Q_{\text{two-phase},i} - Q_{\text{r-coi},i} = 0 \quad (0 < x_i < 1) \tag{29}$$

$$Q_{\text{gas-phase},i} - Q_{\text{r-coi},i} = 0 \qquad (x_i = 1) \tag{30}$$

For the inner surface of copper pipe:

$$Q_{\text{r-coi},i} - Q_{\text{coi-coo},i} = 0 \tag{31}$$

For the outer surface of copper pipe:

$$Q_{\text{coi-coo},i} - Q_{\text{coo-wa},i} = 0 \tag{32}$$

For the water:

$$Q_{\text{coo-wa},i} - Q_{\text{wa-st},i} = 0 \tag{33}$$

For the steel panel channel with copper pipe:

$$Q_{\text{wa-st},i} - Q_{\text{rad-st},i} - Q_{\text{rad-fin},i} - Q_{\text{conv-st},i} - Q_{\text{conv-fin},i} - Q_{\text{conv-fe},i} - Q_{\text{st-stk},i} = 0 \quad (34)$$

For the steel panel channel with water:

$$Q_{\text{st-stk},i} - Q_{\text{rad-stk},i} - Q_{\text{rad-fin},i} - Q_{\text{conv-stk},i} - Q_{\text{conv-fin},i} - Q_{\text{conv-fe},i} = 0 \quad (35)$$

2.4 Economic model

Initial cost is a crucial indicator to evaluate the economic performance of the RDRC terminal, as well as constrained condition for structural optimization. The initial cost (IC) of the RDRC terminal consists of copper pipes cost (IC_{co}), steel panels cost (IC_{st}), fins cost (IC_{fin}) and labor expense (IC_{le}), using Eq. (36). The prices of copper pipes with various diameters are different, which are listed in Table 1. Other material prices and labor expense are also exhibited in Table 1.

$$IC = IC_{\text{co}} + IC_{\text{st}} + IC_{\text{fin}} + IC_{\text{le}} \quad (36)$$

Table 1. The initial cost of the RDRC terminal.

Category	Copper pipe								Steel panel	Fin	Labor expense
Dimension	Outer diameter (mm)								/	/	/
	4.0	5.0	6.35	8.0	9.52	10.0	12.0	14.0			

Unit Cost	0.5	0.9	1.0	1.5	1.6	2.1	2.3	3.5	3.8	0.8	15.1
Unit					$\$\cdot m^{-1}$				$\$\cdot m^{-2}$	$\$\cdot m^{-2}$	\$

2.5 Simulation steps

Based on the above mathematical and economic models, the thermal and economic performances of the RDRC terminal are analyzed with different structural parameters using the Python environment. The simplified calculation flowchart is depicted in Fig. 3 and the detailed version is shown in Appendix C. The operating parameters of the refrigerant mass flow rate G, refrigerant temperature t_r, refrigerant pressure p_r, indoor air temperature t_n, indoor relative humidity φ, airflow velocity v and inlet enthalpy of the refrigerant I_r, as well as structural parameters of the RDRC terminal including total heat transfer area A_t, outer diameter of the copper pipe D_{coo}, copper pipe spacing L_{sp} and fin height H_{fin} are known. The calculation process is as follow: (i) input operating parameters and structural parameters, and then calculate the initial cost of the RDRC terminal IC; (ii) give an initial value of t_{stk}', and calculate the cooling capacity between steel panel channel with copper pipe and steel panel channel with water $Q_{st\text{-}stk,i}$; (iii) calculate the temperature of the steel panel channel with copper pipe $t_{st,i}$ and the cooling capacity of the refrigerant $Q_{two\text{-}phaes,i}$ ($Q_{gas\text{-}phaes,i}$), and then determine the flow state of

the refrigerant x_i ($t_{r,i}$); (iv) calculate the temperature of the steel panel channel with water $t_{stk,i}$ using iteration method until the convergence condition is satisfied, then calculate until i=n and output all values of the t_{coi}, t_{coo}, t_{wa}, t_{st}, t_{stk} and p_r; (v) input different structural parameters and repeat these steps.

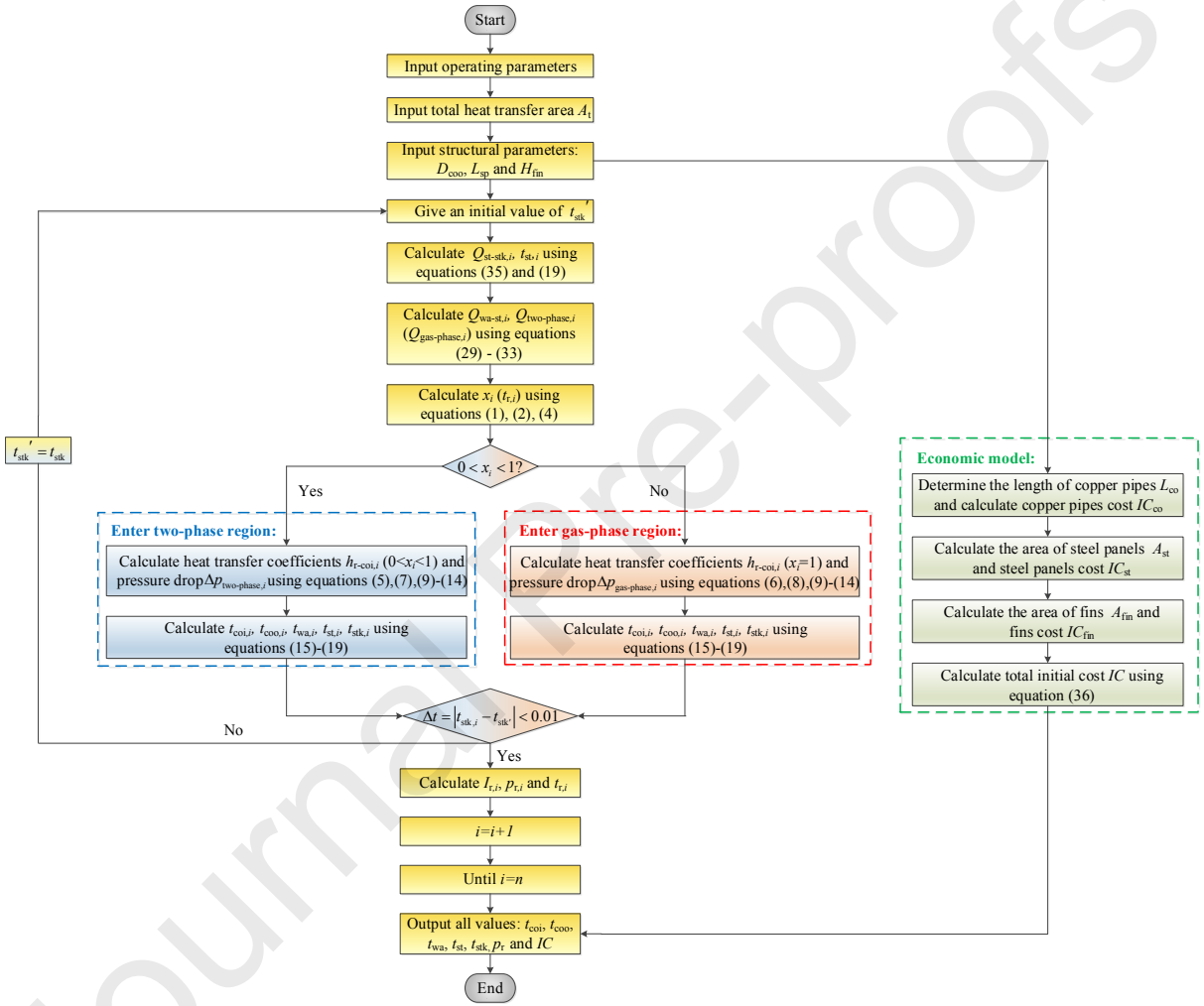

Fig. 3. The simplified calculation flowchart of the RDRC terminal.

3. Experimental system

3.1 System description

The experiments are conducted in a climatic chamber which are composed of outdoor-environmental chamber and indoor-environmental chamber, as shown in Fig. 4. The thermal environments of both chambers can be maintained by their independent control air-conditioning systems. A constructed test room is built in the indoor-environmental chamber to avoid forced convection, with the dimension of 3500 mm (Length) × 3500 mm (Width) × 2500 mm (Height). The RDRC system consists of a compressor, a condenser, a sub-cooler, an electronic expansion valve and the RDRC terminal (evaporator). During the test, the refrigerant is compressed into the high pressure and high temperature states by the compressor and then sent to the condenser. After that, the refrigerant is passed through the sub-cooler and throttled by the electronic expansion valve, and then evaporated by the RDRT terminal. Finally, the refrigerant flows back into the compressor for a new cycle. The refrigerant at the inlet of the RDRC terminal is two-phase state with the vapor quality of 0 ~ 1, and at the outlet is overheated state with the vapor quality of 1. In the experiments, the temperature and relative humidity of the test room are controlled within 22 ~ 30 ^{o}C and 50%. The inlet and outlet

temperatures and pressures of the RDRC terminal and condenser, refrigerant mass flow rate, indoor air temperature, relative humidity and airflow velocity are recorded. The measuring instruments and accuracies are listed in Table 2. The cooling capacity of the RDRT terminal can be calculated according to Eq. (37):

$$Q_{\mathrm{t}}=G\times(I_{\mathrm{out}}-I_{\mathrm{inl}}) \tag{37}$$

where I_{inl} and I_{out} are the inlet and outlet enthalpies of the RDRT terminal, which are obtained by the measured temperature and pressure.

The uncertainties of the experimental results are determined as follows [29]:

$$u_{xi}=\frac{e_i}{k} \tag{38}$$

$$u_y=\sqrt{\sum_{i=1}^{n}\left(\frac{\partial f}{\partial x_i}u_{x_i}\right)^2} \tag{39}$$

where u_{xi} is the uncertainty of x_i, e_i is the maximum error of instrument, k is the coverage factor which is taken as $\sqrt{3}$, and u_y is the uncertainty of u_{xi}. The uncertainties of t, p, G, φ, v and Q_{t} are 1.2%, 5.8%, 1.2%, 2.3%, 3.5% and 2.8%, respectively.

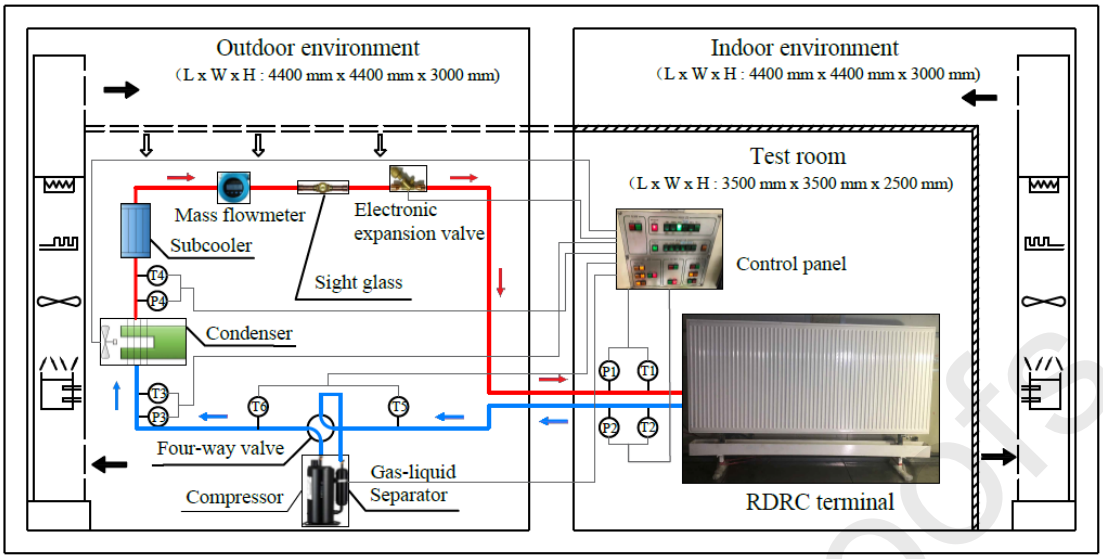

Fig. 4. Schematic diagram of the RDRC system.

Table. 2 Detailed specifications of instruments.

Measured parameter	Instrument	Full scale	Accuracy
temperature	copper-constantan thermocouple	-50 – 150 °C	± 0.5 °C
pressure	pressure transmitter	0 – 45 bar	0.1% FS
refrigerant mass flow rate	mass flowmeter	0 – 100 kg· h^{-1}	± 0.02 kg· h^{-1}
relative humidity	testo humidity sensor	2 – 98% RH	± 2% RH
airflow velocity	TSI-Q-Trak	0 – 40 m· s^{-1}	± 0.02 m· s^{-1}

3.2 Performance analysis of the system

Taking the evaporating temperature of 14 °C, the indoor air temperature of 28 °C and relative humidity of 50% as typical condition, the operating characteristics of the

RDRC system in the steady period are investigated in Fig. 5. It can be found that the evaporating temperature is approximately 0.6 °C lower than the water temperature and 1.5 °C lower than the RDRC terminal surface temperature. This is attributed to the existence of the water between copper pipes and steel panels. The average temperature of the RDRC terminal surface is 15.5 °C, within a fluctuation merely ±0.2 °C, which indicates that the temperature distribution of the RDRC terminal surface is homogenous. The temperature difference between fin-base and fin-end is around 1 °C. The fluctuation range of condensing temperature is 39.9 °C ~ 40.3 °C, the range of refrigerant mass flow rate is 4.08×10^{-3} ~ 4.12×10^{-3} kg·s^{-1}, and the range of water condensation rate is 4.7 $\times10^{-5}$~ 5.1×10^{-5} kg·s^{-1}. During the operation, the indoor air temperature remains 27.9 °C consistently, illustrating that the RDRC system has excellent stability.

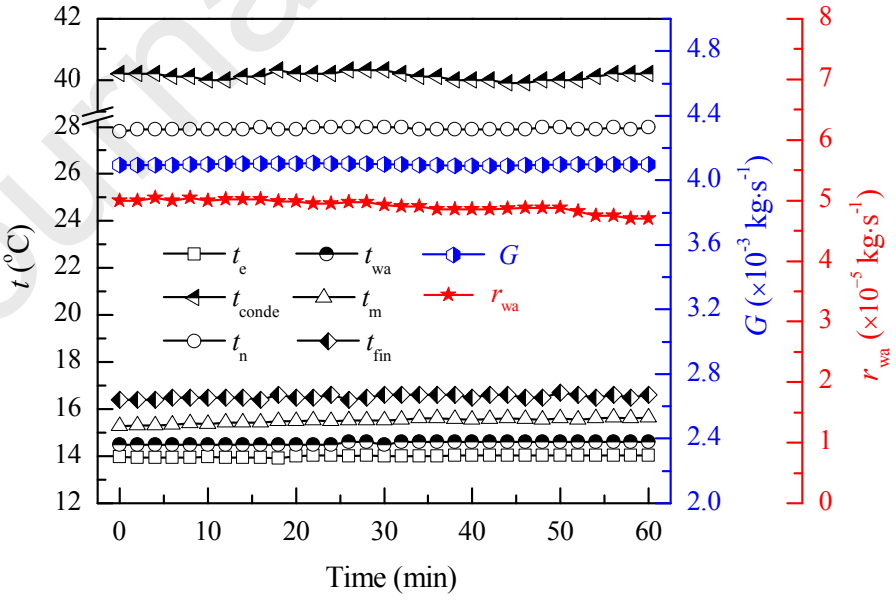

Fig. 5. The operating characteristics of the RDRC system.

Fig. 6 shows the effects of evaporating temperature and indoor air temperature on thermal performance of the RDRC terminal. With the increase of the indoor air temperature, the RDRC terminal surface temperature ascends. It can be ascribed that the difference between evaporating temperature and indoor air temperature rises, and the evaporation rate of refrigerant goes up, and then the refrigerant outlet superheat increases. Meanwhile, the refrigerant outlet temperature is improved, leading to the enhancement of the RDRC terminal surface temperature. Besides, the RDRC terminal surface temperature shows an increasing trend when the evaporating temperature varies from 6.1 ^{o}C to 14.2 ^{o}C. This is attributed to the improvement of the copper pipes temperature and the water temperature. When the evaporating temperature remains a certain value, the maximum difference between the RDRC terminal surface temperature and evaporating temperature is not exceed 3.1 ^{o}C, indicating that the heat transfer resistance of the RDRC terminal is petty. Furthermore, the horizontal radiation asymmetry of the RDRC system is depicted in Fig 6. It can be found that the *PDs* descend with the rise of the evaporating temperature due to the reduction of the difference between the mean radiant temperature of interior wall with RDRC terminal and the mean radiant temperature of the opposite wall. The maximum *PD* value is 0.6 under the condition of the evaporating temperature with 6.1 ^{o}C and indoor air

temperature with 30 °C, which can meet the thermal comfort level of Class A (less than 5) [30]. Therefore, it can be concluded that the RDRC system is acceptable to occupants in terms of horizontal radiation asymmetry.

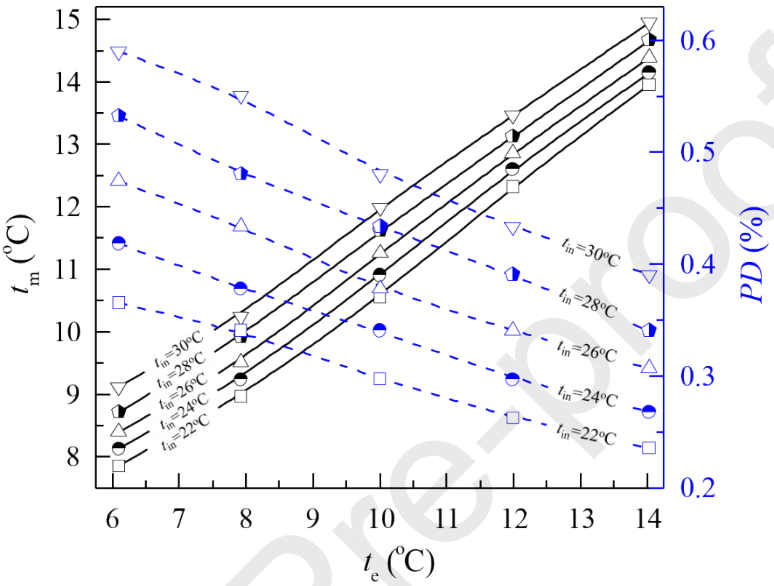

Fig. 6. Temperature distribution and horizontal radiation asymmetry of the RDRC system.

3.3 Model validation

The structural parameters of the RDRC terminal are listed in Table 3. The comparisons of the measured data and simulated results of the RDRC system are presented in Table 4. Cases 1 ~ 5 reflect the thermal performance of this system at different evaporating temperatures, under the indoor air temperature of 26 °C. Cases 6 ~ 10 and Cases 11 ~ 15 reflect its thermal performance under the indoor air temperature of 28 °C and 30 °C. It can be observed that the mean and maximum deviations of the

refrigerant outlet temperature are 0.4 °C and 0.7 °C, and 0.6 °C and 1.1 °C for the mean surface temperature of the RDRC terminal. The relative errors of the refrigerant outlet pressure and the total cooling capacity of this system are 0.8% ~ 7.9% and 0.1% ~ 0.7%, respectively. All the deviation values are acceptable, which indicates that the constructed mathematical model can accurately evaluate the thermal performance of the RDRC system.

Table 3. The structure parameters of the RDRC terminal.

Parameters	Dimension (mm)	Parameters	Dimension (mm)
RDRC terminal length	2000.0	inner diameter of copper pipe	5.35
RDRC terminal width	100.0	outer diameter of copper pipe	6.35
RDRC terminal height	900.0	fin length	30.0
copper pipe length	60000.0	fin spacing	10.0
copper pipe spacing	60.0	fin thickness	1.0

Table 4. Measured data and simulated results of the RDRC system.

Case	t_n (°C)	t_e (°C)	G ($\times 10^{-3}$ kg· s^{-1})	$p_{r\text{-}inl}$ ($\times 10^6$ Pa)	$t_{r\text{-}inl}$ (°C)	$p_{r\text{-}out,test}$ ($\times 10^6$ Pa)	$p_{r\text{-}out,sim}$ ($\times 10^6$ Pa)	$t_{r\text{-}out,test}$ (°C)	$t_{r\text{-}out,sim}$ (°C)	$t_{m,test}$ (°C)	$t_{m,sim}$ (°C)	$Q_{t\text{-}test}$ (W)	$Q_{t\text{-}sim}$ (W)
1	26.0	14.0	13.1	1.24	14.9	1.20	1.21	17.4	18.0	16.9	17.5	2186.4	2184.9
2	26.0	12.1	13.6	1.19	13.4	1.12	1.15	17.1	17.2	16.0	16.3	2288.5	2283.2
3	26.0	10.2	14.2	1.13	12.0	1.05	1.08	16.7	16.9	14.9	15.3	2379.9	2382.1
4	26.0	8.1	14.7	1.08	10.4	0.97	1.02	16.1	16.4	13.8	14.5	2471.7	2469.2
5	26.0	6.1	15.3	1.03	8.8	0.90	0.96	15.4	15.6	12.7	13.6	2574.6	2567.2
6	28.0	14.0	13.2	1.24	14.8	1.20	1.21	19.0	19.5	17.6	18.1	2229.6	2237.6
7	28.0	12.0	13.7	1.18	13.3	1.12	1.14	18.5	18.9	16.6	17.0	2322.8	2331.4
8	28.0	10.0	14.4	1.13	11.5	1.04	1.08	18.1	18.4	15.6	16.1	2441.9	2445. 6
9	28.0	8.1	14.9	1.08	10.7	0.97	1.02	17.7	17.8	14.7	15.2	2528.5	2512.8
10	28.0	6.1	15.4	1.03	8.9	0.90	0.96	17.1	17.8	13.6	14.7	2602.6	2611.9
11	30.0	14.2	13.4	1.25	15.1	1.20	1.21	21.3	21.5	18.7	19.3	2292.9	2303.0
12	30.0	12.0	14.2	1.19	13.2	1.11	1.14	20.7	20.8	17.7	18.1	2423.1	2426.1
13	30.0	10.0	14.7	1.13	11.8	1.04	1.08	20.3	20.9	16.9	17.4	2509.6	2527.2
14	30.0	8.1	15.1	1.08	10.4	0.97	1.02	19.7	20.1	16.2	16.5	2591.9	2604.8
15	30.0	5.9	15.4	1.03	8.8	0.89	0.96	18.3	19.0	14.6	15.2	2623.9	2638.6

4. Results and analysis

4.1 Performance analysis of the RDRC terminal

When the surface area of the RDRC terminal keeps constant at the value of 25.2 m^2, the effects of different structural parameters including fin height, copper pipe diameter and copper pipe spacing on thermal and economic performances of this system are investigated. Then the length of copper pipes is regulated to meet the requirements of different structure conditions of this terminal. The operating parameters are remained as:

$$G = 1.67 \times 10^{-2}\ \text{kg}\cdot\ \text{s}^{-1},\ t_r = 12\ ^{o}\text{C},\ p_r = 1.1\times 10^{6}\ \text{Pa},\ t_n = 26\ ^{o}\text{C},$$

$$\varphi = 60\%,\ v = 0.2\ \text{m}\cdot\ \text{s}^{-1},\ I_r = 2.6\times 10^{5}\ \text{J}\cdot\ \text{kg}^{-1},\ \Delta l = 0.05$$

4.1.1 Effect of the fin height

When the copper pipe diameter D_{coo} is 6.0 mm and copper pipe spacing L_{sp} is 60.0 mm, the effect of the fin height H_{fin} on thermal performance of the RDRC terminal is illustrated in Fig. 7. With the increase of the H_{fin}, the cooling capacity for per exterior area Q_{ea} improves rapidly then slowly. On the contrary, the length of the copper pipes L_{co}, the mean surface temperature of the RDRC terminal t_m and the fin efficiency η_{fin} are diminished. The Q_{ea} varies from 808.9 W to 1390.5 W due to the decrease of the t_m,

leading to the enhancement of the heat transfer between the RDRC terminal surface and indoor environment. The t_m descends from 16.9 °C to 14.1 °C, which is ascribed that the L_{co} decreases, and the refrigerant outlet overheat mitigates, resulting in the reduction of the refrigerant outlet temperature. The η_{fin} drops from 94.6% to 63.8% due to the increment of the mean surface temperature of the fin. With regard to Fig. 8, the pressure drop of the refrigerant Δp_r shows a trend of declining first and then flattening with the rise of the H_{fin} as for the diminution of the L_{co}. The economic performance of the RDRC terminal with different H_{fin} is also exhibited in Fig. 8. It is found that the *IC* varies from 187.6 $ to 114.5 $ because the change rate of the IC_{co} is superior to the IC_{fin}, indicating that the IC_{co} plays a prominent role in the *IC*. When the H_{fin} is larger than 40.0 mm, the H_{fin} has an insignificant influence on the Q_{ea}. Besides, the Q_{ea} cannot meet the requirements for occupants under the condition of the H_{fin} with 10.0 mm ~ 20.0 mm. Therefore, it is advisable to set the H_{fin} within the range of 20.0 mm ~ 40.0 mm for optimizing the structural parameters of the RDRC terminal.

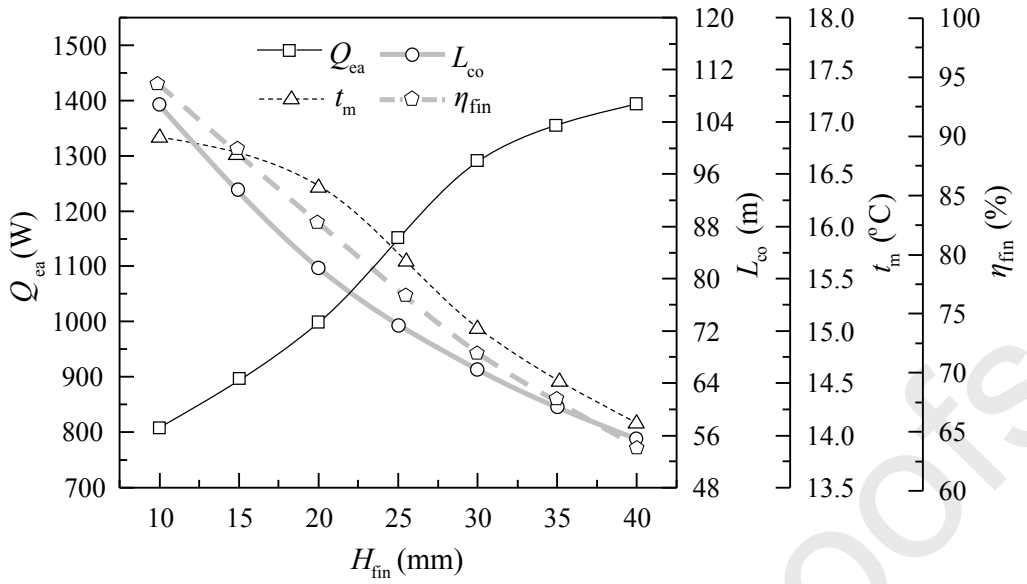

Fig. 7. Effect of the H_{fin} on thermal performance of the RDRC terminal.

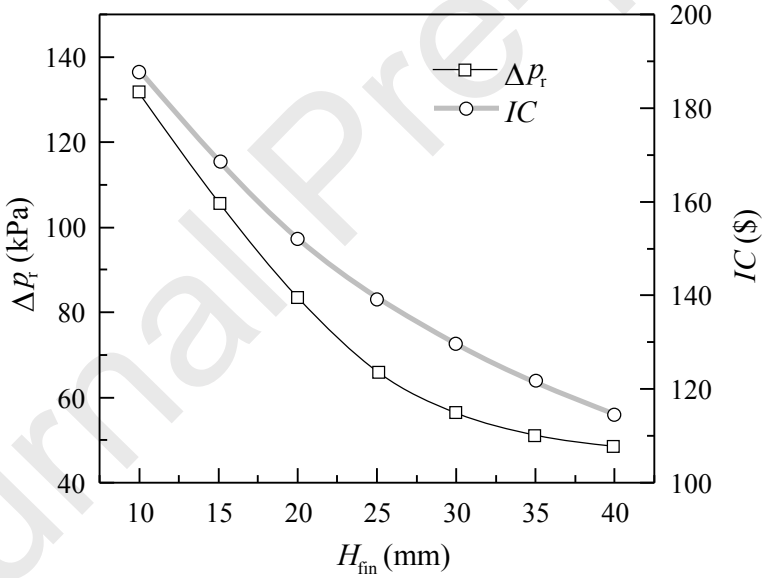

Fig. 8. Effect of the H_{fin} on economic performance of the RDRC terminal.

4.1.2 Effect of the copper pipe diameter

Under the condition of the L_{sp} with 60.0 mm and H_{fin} with 30.0 mm, the variation trends of the thermal performance of the RDRC terminal with the D_{coo} are depicted in Fig. 9. With the rise of the D_{coo}, both the Q_{ea} and L_{co} are descended, while the t_m ascends significantly. The Q_{ea} decreases from 1438.3 W to 1152.5 W when the D_{coo} varies from 5.0 mm to 14.0 mm. It is attributed to the reduction of the L_{co} that varies from 61.2 m to 53.6 m. The t_m increases from 16.6 °C to 17.3 °C since the surface area of the copper pipes raises, and the convective heat transfer between refrigerant and copper pipes descends, and then the copper pipes temperature increases, resulting in the depression of the heat transfer between copper pipes and RDRC terminal surface. As shown in Fig. 10, with the increase of the D_{coo}, the Δp_r drops rapidly then slowly due to the mitigation of the refrigerant flow rate in copper pipes. The effect of the D_{coo} on economic performance of the RDRC terminal is also illustrated in Fig. 10. With the increase of the D_{coo}, the *IC* elevates dramatically and its average growth rate is 9.3% as for the improvement of the IC_{co}. When the D_{coo} is larger than 7.0 mm, the Q_{ea} decreases gradually while the *IC* is increasing continuously with uneconomical performance. Therefore, the D_{coo} of the 5.0 mm ~ 7.0 mm is a good choice for optimizing structural parameters of the RDRC terminal.

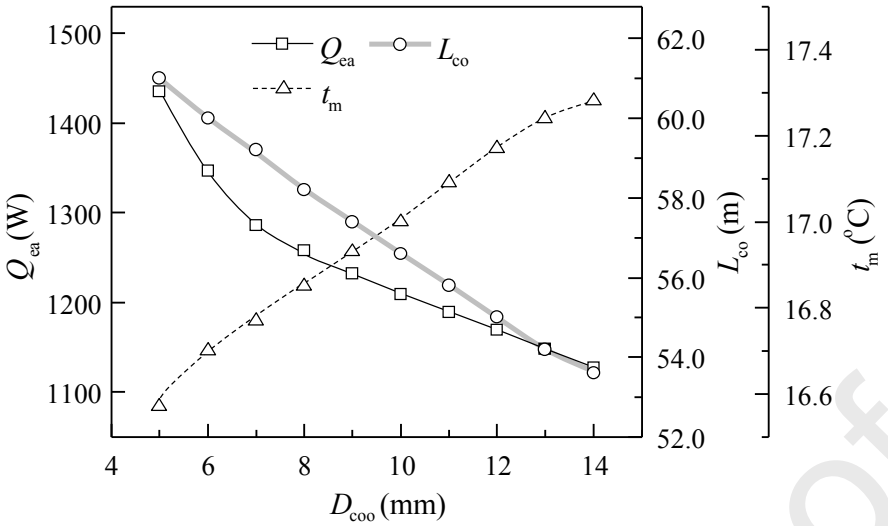

Fig. 9. Effect of the D_{coo} on thermal performance of the RDRC terminal.

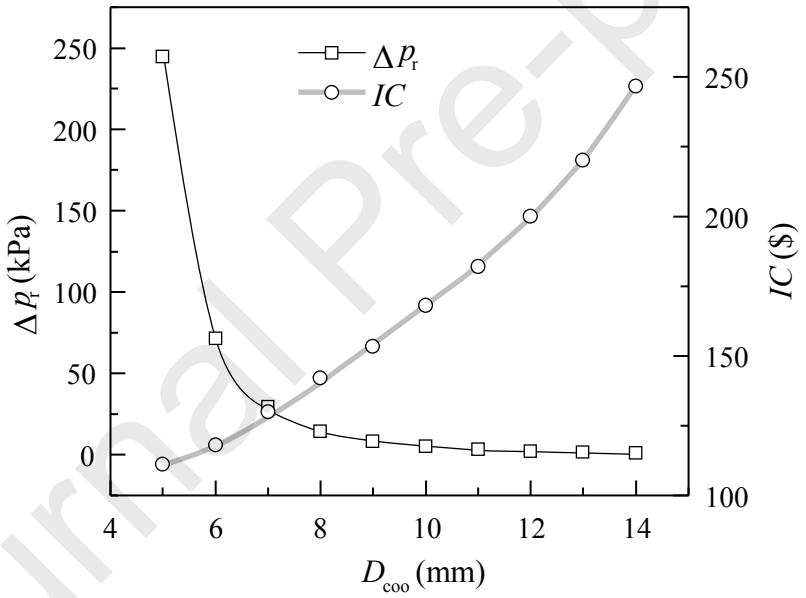

Fig. 10. Effect of the D_{coo} on economic performance of the RDRC terminal.

4.1.3 Effect of the copper pipe spacing

Figs. 11 and 12 present the changes of the thermal and economic performances of

the RDRC terminal with different L_{sp}, given that the D_{coo} remains 6.0 mm and H_{fin} remains 30.0 mm. With the increase of the L_{sp}, the Q_{ea}, L_{co} and Δp_r decreases, while the t_m ascends slightly. When the L_{sp} ascends from 40.0 mm to 100.0 mm, the t_m varies from 16.7 °C to 16.9 °C. This can be explained by the increment of the steel panel areas and the reduction of the temperature difference between refrigerant and steel panels. The Q_{ea} descends since the t_m improves and the exterior area of the RDRC terminal enhances. The variation of the Δp_r is within the range of 6.8×10^4 Pa ~ 3.9×10^4 Pa due to the reduction of the L_{co} (66.4 m ~ 50.4 m). In addition, the *IC* reveals a decline trend, which can be ascribed that the decline degree of the IC_{co} is higher than the growth degree of the IC_{st} in spite of the enhancement of the steel panel areas. In order to provide enough cooling capacity of the RDRC terminal, the L_{sp} with 40.0 mm ~ 80.0 mm is selected for structural optimization.

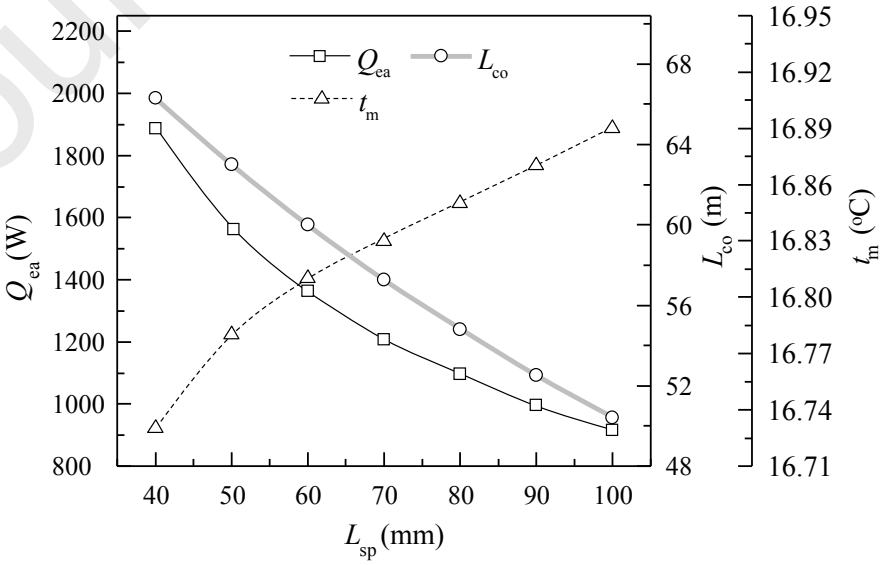

Fig. 11. Effect of the L_{sp} on thermal performance of the RDRC terminal.

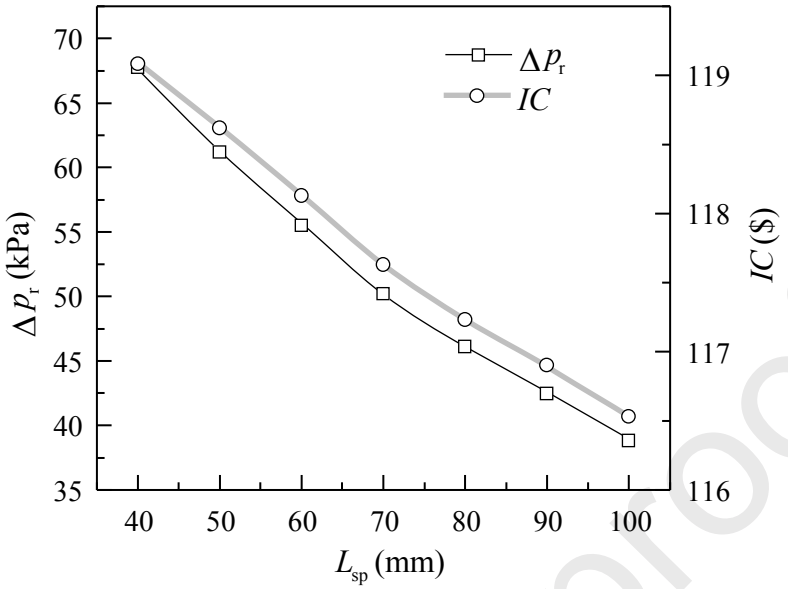

Fig. 12. Effect of the L_{sp} on economic performance of the RDRC terminal.

4.2 Optimal design of the RDRC terminal

Orthogonal design is a scientific method to deal with multi-factor experiments, which adopts the standardized orthogonal table for arranging the test reasonably [31]. With this method, it is beneficial to reduce test times and judge superior conditions and can grasp the test results more comprehensively and systematically through statistical analysis and then determine the optimum schemes [32]. In this study, the structural parameters of the RDRC terminal are optimized by orthogonal design method. Based on the aforementioned analysis, the structural parameters of the H_{fin}, D_{coo} and L_{sp} have great significances on thermal and economic performances of the RDRC terminal.

Hence, these variables are taken as impact factors and their corresponding levels are exhibited in Table 5. The standard orthogonal table of L_9 (3^4) is selected since each factor contains three levels. The cooling capacity for per exterior area of the RDRC terminal Q_{ea} is considered as objective function and the IC < 121.1 $ is taken as constraint condition.

Table 5. Factors and corresponding levels list of orthogonal test.

Factor levels	A H_{fin} (mm)	B D_{coo} (mm)	C L_{sp} (mm)
1	20.0	5.0	40.0
2	30.0	6.0	60.0
3	40.0	7.0	80.0

The optimal results of orthogonal test are illustrated in Table 6. The range R' value of the L_{sp} is the largest, the range R' value of the H_{fin} is the second, and range R' value of the D_{coo} is the smallest. It is indicated that the influencing degree of these factors is as follow: $L_{sp} > H_{fin} > D_{coo}$. Test 8 shows the best thermal performance of the RDRC terminal: the H_{fin} is 40.0 mm, the D_{coo} is 6.0 mm, the L_{sp} is 40.0 mm and the Q_{ea} attains 2199.1 W· m^{-2}. Correspondingly, Test 3 shows the worst thermal performance of the RDRC terminal: the H_{fin} is 20.0 mm, the D_{coo} is 7.0 mm, the L_{sp} is 80.0 mm and the Q_{ea} is merely 906.6 W· m^{-2}. According to the calculation and analysis of orthogonal test, the optimal level of the structural parameters is the H_{fin} with 30.0 mm, the D_{coo} with 5.0

mm and the L_{sp} with 40.0 mm ($A_2B_1C_1$). However, the Q_{ea} of the optimal level is 1986.7 W· m^{-2}, which is less than the Test 8. While the *IC* of the optimal level is higher than the Test 8, with a fluctuation 7.2 $. Therefore, considering the thermal and economic performances of the RDRC terminal, the structural parameters of the H_{fin} with 40.0 mm, the D_{coo} with 6.0 mm and the L_{sp} with 40.0 mm can be adopted in future application.

Table 6. Test results analysis of orthogonal design method.

Test number	A	B	C	Objective function	Constraint condition
	H_{fin} (mm)	D_{coo} (mm)	L_{sp} (mm)	Q_{ea} (W· m^{-2})	*IC* ($)
1	1 (20.0)	1 (5.0)	1 (40.0)	1583.6	135.5
2	1 (20.0)	2 (6.0)	2 (60.0)	1129.7	140.9
3	1 (20.0)	3 (7.0)	3 (80.0)	906.6	154.2
4	2 (30.0)	1 (5.0)	2 (60.0)	1431.9	113.7
5	2 (30.0)	2 (6.0)	3 (80.0)	1077.0	119.9
6	2 (30.0)	3 (7.0)	1 (40.0)	1784.2	138.3
7	3 (40.0)	1 (5.0)	3 (80.0)	1296.2	101.4
8	3 (40.0)	2 (6.0)	1 (40.0)	2199.1	106.6
9	3 (40.0)	3 (7.0)	2 (60.0)	1510.8	119.8
K_1	3619.9	4311.7	5566.8	/	/
K_2	4293.1	4405.8	4072.4	/	/
K_3	5006.1	4201.6	3279.8	/	/
k_1	1206.6	1437.2	1855.6	/	/
k_2	1431.0	1468.6	1357.5	/	/
k_3	1668.7	1400.5	1093.3	/	/
R'	462.1	68.1	762.3	/	/
Optimal level	A_2	B_1	C_1	1986.72	113.8
Order		C > A > B		/	/

4.3 Comparisons of different aspect ratio

Based on the optimal structural parameters and the length of the copper pipes in Test 8, the calculated exterior area of the RDRC terminal is 1.26 m^2. In order to investigate the effect of the aspect ratio *L/H* on thermal and economic performances of this terminal, different structural forms of the *L/H* with 0.56, 0.88, 1.56 and 3.50 are designed, as shown in Fig. 13. The operating parameters are unchanged and the comparison results of different aspect ratios are depicted in Fig. 14. It can be found that with the increase of the *L/H*, the Q_{ea} decreases with the drop rate of 5.5%, which is attributed to the reduction of the L_{co}. Correspondingly, the *IC* is declined as well. Type A presents the best thermal performance; however, the *IC* (125.1 $) is larger than the constraint condition. Thus, type B is a more preferable choice considering the thermal and economic performances of the RDRC terminal. From the perspective of thermal comfort, the RDRC terminal with higher height is conductive to exchange heat with indoor environment sufficiently due to the sinking of cold air. Therefore, the RDRC terminal with type B can create a more comfortable indoor thermal environment than the RDRC terminal with type C and D.

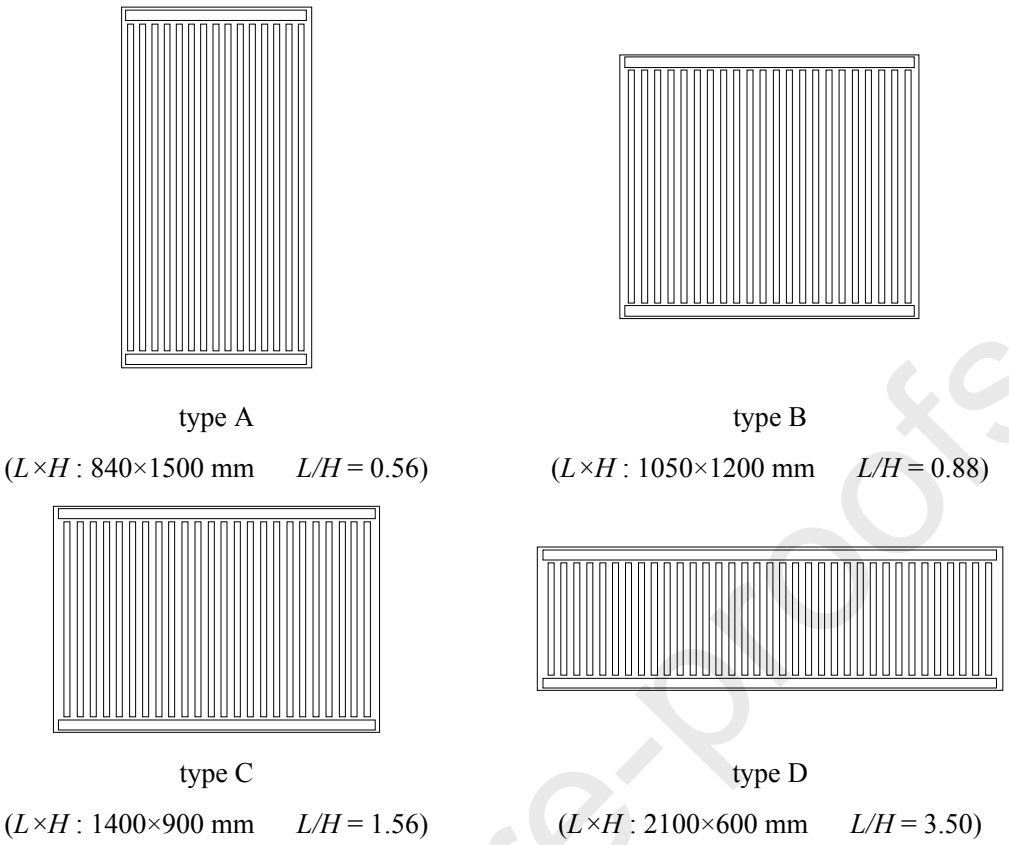

Fig. 13. The RDRC terminal with different aspect ratios.

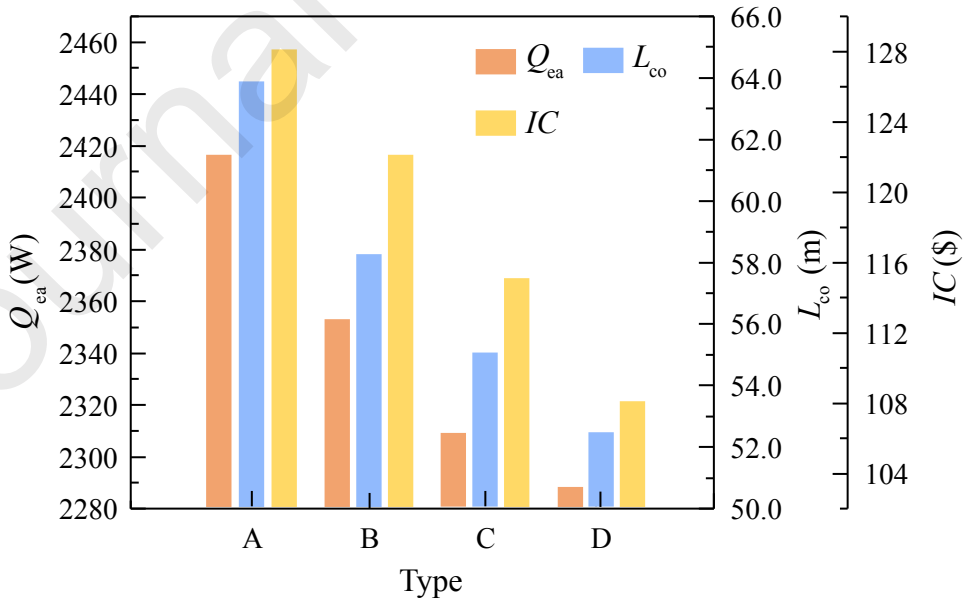

Fig. 14. Effect of the *L/H* on thermal and economic performances of the RDRC terminal.

5. Discussion

The proposed RDRC system provides cooling by the combination of radiation and natural convection, and the total cooling capacity of the optimal structure is 2964.8 W at the indoor air temperature of 26 ^{o}C and relative humidity of 60%. Regarding to the fan coil system which depends on forced convection only, and its cooling capacity is 3520 W under the same condition [33]. It indicates that the RDRC system is inferior to the fan coil system in terms of cooling performance. However, the RDRC system has its own superiority on indoor thermal comfort due to its no draught sensation and fan noise, which exhibits widely promising applications.

6. Conclusion

To conquer the defects of split air-conditioners and radiant cooling systems, a novel RDRC system is proposed in this paper. Experiments are conducted to evaluate the thermal performance of this system. The mathematical and economic models of the RDRC terminal are developed and the mathematical model is validated with the experimental results. The impacts of the structural parameters including fin height, copper pipe diameter, copper pipe spacing and aspect ratio on thermal and economic

performances of this terminal are investigated. Based on the orthogonal design method, the sequencing of the impact factors and the optimal structure of this terminal are obtained. The main conclusions are given as follows:

(1) During the stable period, the average temperature of the RDRC terminal surface is 15.5 ^{o}C, within a fluctuation merely ±0.2 ^{o}C, which indicates that the temperature distribution of this terminal surface is quite homogenous and this system has the potential of creating stable thermal environment. Besides, the RDRC system has the characteristics of independent dehumidification and the mean water condensation rate of this terminal is 4.9×10^{-5} kg·s^{-1}.

(2) The constructed mathematical model is validated to be reliable and can accurately evaluate the thermal performance of the RDRC system. The relative errors of the refrigerant outlet temperature and pressure, the RDRC terminal surface temperature and the total cooling capacity of this system are 0.5% ~ 4.1%, 0.8% ~ 7.9%, 1.9% ~ 8.1% and 0.1% ~ 0.7%, respectively.

(3) The impact degree of three factors is copper pipe spacing, fin height and copper pipe diameter in turns. When the surface area of the RDRC terminal keeps 25.2 m^2, the optimal structure of this terminal is the fin height with 40.0 mm, the copper pipe diameter with 6.0 mm and the copper pipe spacing with 40.0 mm.

(4) The aspect ratio means the ratio of length to width of the RDRC terminal. When the aspect ratio varies from 0.56 to 3.50, both the cooling capacity for per exterior area and initial cost of this terminal are decreased. In view of the thermal and economic performances of the RDRC terminal, type B (aspect ratio with 0.88) is the optimal structure.

Acknowledgements

This work was supported by the National Natural Science Foundation of China (No. 52008290).

Appendix A

Regarding to the convective heat transfer coefficient of the refrigerant, h_{l} can be calculated by Chen [34], and h_{pb} is derived from the formula as presented by Cooper [35]:

$$h_{\mathrm{l}} = 0.023 \cdot Re_{\mathrm{l}}^{0.8} Pr_{\mathrm{l}}^{0.4} \frac{\lambda_{\mathrm{l}}}{D_{\mathrm{r}}} \tag{40}$$

$$h_{\mathrm{pb}} = 55 q^{2/3} \left(\frac{p}{p_c}\right)^{0.12} \left(-\lg \frac{p}{p_c}\right)^{-0.55} \cdot M^{-0.5} \tag{41}$$

$$E = 1 + 24000 \cdot Bo^{1.16} + 1.37 \cdot X_{tt}^{-0.86} \tag{42}$$

$$S = \frac{1}{1 + 1.15 \times 10^{-6} \cdot E^2 \cdot Re_{\mathrm{l}}^{1.17}} \tag{43}$$

$$Re_{\mathrm{l}} = \frac{G(1-x) \cdot D_{\mathrm{r}}}{\mu_{\mathrm{l}}}, \quad Re_{\mathrm{g}} = \frac{G \cdot D_{\mathrm{r}}}{\mu_{\mathrm{g}}} \tag{44}$$

$$Pr_{\mathrm{l}} = \frac{\mu_{\mathrm{l}} c_{p\mathrm{l}}}{\lambda_{\mathrm{l}}}, \quad Pr_{\mathrm{g}} = \frac{\mu_{\mathrm{g}} c_{p\mathrm{g}}}{\lambda_{\mathrm{g}}} \tag{45}$$

$$Bo = \frac{q}{G \Delta h_{\mathrm{lv}}} \tag{46}$$

$$X_{tt} = \left(\frac{1-x}{x}\right)^{0.9} \left(\frac{\rho_{\mathrm{g}}}{\rho_{\mathrm{l}}}\right)^{0.5} \left(\frac{\mu_{\mathrm{l}}}{\mu_{\mathrm{g}}}\right)^{0.1} \tag{47}$$

where Re_{l} and Pr_{l} are the Reynolds number and Prandtl number of the refrigerant in liquid state; λ_{l} is the thermal conductivity of the refrigerant in liquid state; q is the heat flux of the refrigerant; p and p_c are the pressure and critical pressure of the refrigerant; M is the molecular weight of the refrigerant; Bo is the boiling number; X_{tt} is the Martinelli parameter; μ_{l} and μ_{g} are the dynamic viscosities of the refrigerant in liquid and gas states; $c_{p\mathrm{l}}$ is the specific heat of the refrigerant in liquid state; Δh_{lv} is the latent heat of vaporization; ρ_{l} and ρ_{g} are the densities of the refrigerant in liquid and gas states.

Appendix B

The natural convective heat transfer coefficient between steel panels and indoor space, h_{air} can be determined as:

$$h_{\text{air}} = \frac{Nu \cdot \lambda_{\text{air}}}{\Delta l} \tag{48}$$

$$Nu = 0.59 \cdot (Gr \cdot Pr)^{1/4} \quad 10^4 < Gr \cdot Pr < 10^9 \tag{49}$$

$$Nu = 0.59 \cdot (Gr \cdot Pr)^{1/4} \quad 10^9 < Gr \cdot Pr < 10^{13} \tag{50}$$

$$Gr = \frac{g_a \alpha \Delta t (\Delta l)^3}{v^2}, \quad Pr = \frac{c_{p-\text{air}} \mu}{\lambda_{\text{air}}} \tag{51}$$

where Nu is the Nusselt number of natural convection; λ_{air} is the thermal conductivity of air; Gr is the Grashof number of air; Pr is the Prandtl number of air; α is the volume expansion coefficient; Δt is the temperature difference between air and steel panels; v is the kinematic viscosity of air; μ is the dynamic viscosity of air.

Appendix C

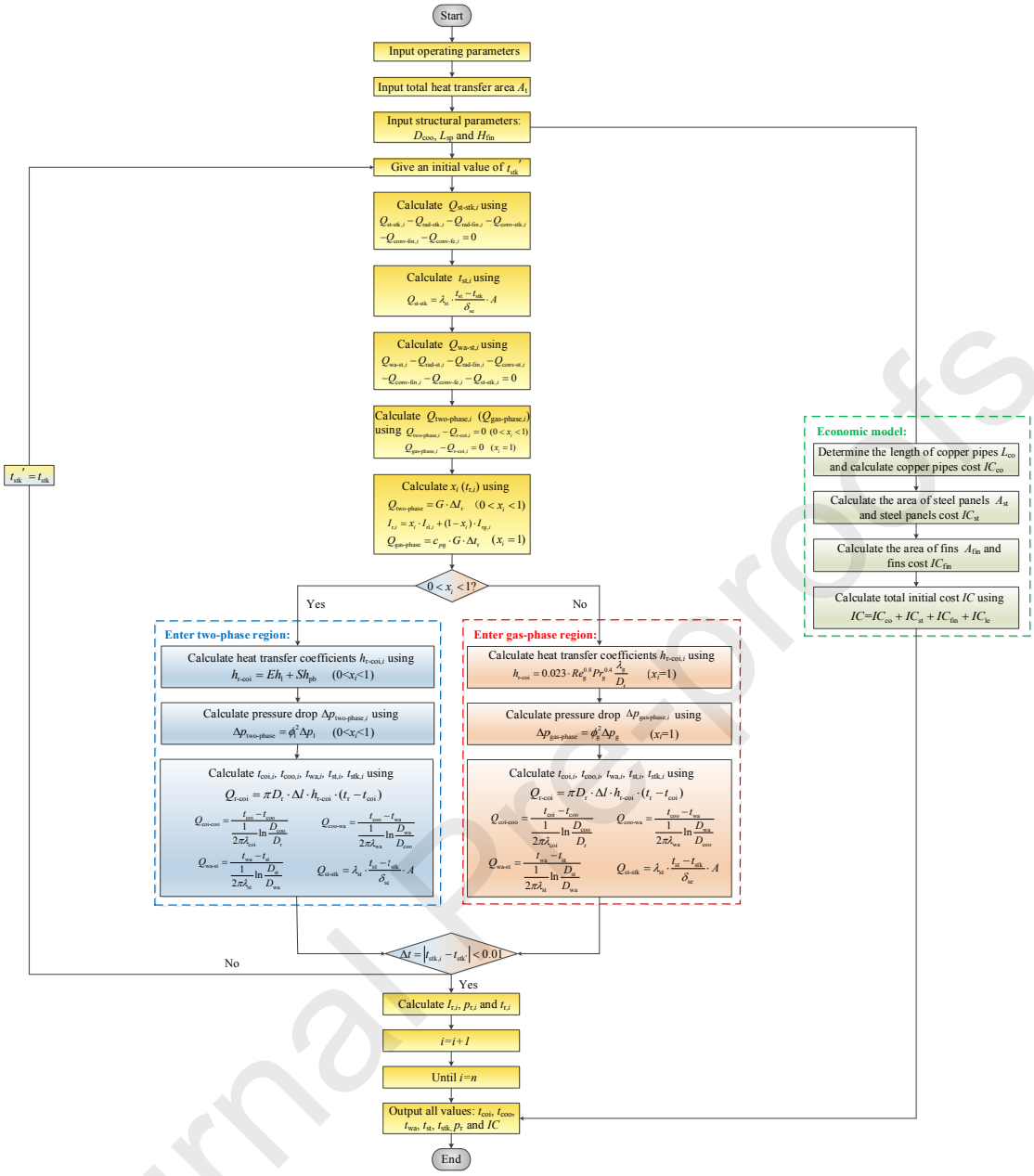

Fig. 3. The detailed calculation flowchart of the RDRC terminal.

References

[1] G. Lv, C. Shen, Z. Han, W. Liao, D. Chen, Experimental investigation on the cooling performance of a novel grooved radiant panel filled with heat transfer liquid, Sustain. Cities. Soc. 50 (2019) 101638. https://doi.org/10.1016/j.scs.2019.101638.

[2] J.L. Dréau, P. Heiselberg, Sensitivity analysis of the thermal performance of radiant and convective terminals for cooling buildings, Energ. Buildings 82 (2014) 482–491. http://dx.doi.org/10.1016/j.enbuild.2014.07.002.

[3] J. Pantelic, S. Schiavon, B. Ning, E. Burdakis, P. Raftery, F. Bauman, Full scale laboratory experiment on the cooling capacity of floor system, Energ. Buildings 170 (2018) 134-144. https://doi.org/10.1016/j.enbuild.2018.03.002.

[4] T. Catalina, J. Virgone, F. Kuznik, Evaluation of thermal comfort using combined CFD and experimentation study in a test room equipped with a cooling ceiling, Build. Environ. 44 (2009) 1740-1750. https://doi.org/10.1016/j.buildenv.2008.11.015.

[5] K. Kitagawa, N. Komoda, H. Hayano, S.-i. Tanabe, Effect of humidity and small air movement on thermal comfort under a radiant cooling ceiling by subjective experiments, Energ. Buildings 30 (1999) 185-193. https://doi.org/10.1016/S0378-7788(98)00086-3.

[6] J.L. Niu, L.Z. Zhang, H.G. Zuo, Energy savings potential of chilled-ceiling combined with desiccant cooling in hot and humid climates, Energ. Buildings 34 (2002) 487-495. https://doi.org /10.1016/S0378-7788(01)00132-3.

[7] P. Peng, G. Gong, X. Mei, J. Liu, F. Wu, Investigation on thermal comfort of air carrying energy radiant air-conditioning system in south-central China, Energ. Buildings 182 (2019) 51-60. https://doi.org/10.1016/j.enbuild.2018.10.020.

[8] Y.Z. Xia, S.A. Mumma, Ceiling radiant cooling panels employing heat-conducting rails: Deriving the governing heat transfer equations, ASHRAE Transactions, 112(1) (2006) 34-41.

[9] Q.Q. Li, C. Chen, Y. Zhang, J. Lin, H.S. Ling, Y. Ma, Analytical solution for heat transfer in a multilayer floor of a radiant floor system, Build. Simul-China 7(3) (2014) 207-216. https://doi.org/10.1007/s12273-013-0152-5.

[10] Z. Tian, X.L. Yin, Y. Ding, C. Zhang, Research on the actual cooling performance of ceiling

radiant panel, Energ. Buildings 47 (2012) 636-642. https://doi.org/10.1016/j.enbuild.2012.01.005.

[11] Y.Q. Luo, L. Zhang, Z.B. Liu, Y.Z. Wang, F.F. Meng, L. Xie, Modeling of the surface temperature field of a thermoelectric radiant ceiling panel system, Appl. Energy 162 (2016) 675-686. https://doi.org/10.1016/j.apenergy.2015.10.139.

[12] L. Shen, Z. Tu, Q. Hu, C. Tao, H. Chen, The optimization design and parametric study of thermoelectric radiant cooling and heating panel, Appl. Therm. Eng. 112 (2017) 688-697. https://doi.org/10.1016/j.applthermaleng.2016.1.

[13] X. Su, L. Zhang, Z. Liu, Y. Luo, J. Lian, Y. Luo, A computational model of an improved cooling radiant ceiling panel system for optimization and design, Build. Environ. 163 (2019) 106312. https://doi.org/10.1016/j.buildenv.2019.106312.

[14] M. Mosa, M. Labat, S. Lorente, Role of flow architectures on the design of radiant cooling panels, a constructal approach, Appl. Therm. Eng. 150 (2019) 1345-1352. https://doi.org/10.1016/j.applthermaleng.2018.1.

[15] H. Lim, Y.-K. Kang, J.-W. Jeong, Thermoelectric radiant cooling panel design: Numerical simulation and experimental validation, Appl. Therm. Eng. 144 (2018) 248-261. https://doi.org/10.1016/j.applthermaleng.2018.0.

[16] H. Tang, X.-H. Liu, Y. Jiang, Theoretical and experimental study of condensation rates on radiant cooling surfaces in humid air, Build. Environ. 97 (2016) 1-10. https://doi.org/10.1016/j.buildenv.2015.12.003.

[17] H. Wang, H. Shu, L. Duanmu, A Review on Radiant Cooling System in Buildings of China, Springer Berlin Heidelberg, 2014.

[18] B. Ning, Y. Chen, H. Liu, S. Zhang, Cooling capacity improvement for a radiant ceiling panel with uniform surface temperature distribution, Build. Environ. 102 (2016) 64-72. https://doi.org/10.1016/j.buildenv.2016.03.009.

[19] C.W. Xu, G.C. Gong, H.W Yang, S.Y. Gong, Numerical study of moisture condensation on pore panels of air-carrying energy radiation air-conditioning system, Building Science 30 (2014) 79-84.

[20] F. Fernández Hernández, J.M. Cejudo López, A. Fernández Gutiérrez, F. Domínguez Muñoz, A new terminal unit combining a radiant floor with an underfloor air system: Experimentation and numerical model, Energ. Buildings 133 (2016) 70-78. https://doi.org/10.1016/j.enbuild.2016.09.040.

[21] L.Z. Zhang, J.L. Niu, Indoor humidity behaviors associated with decoupled cooling in hot and humid climates, Build. Environ. 38 (2003) 99-107. https://doi.org/10.1016/S0360-1323(02)00018-5.

[22] X. Sui, X. Zhang, X. Han, Performance analysis on a residential radiant chilled ceiling system and evaluation on indoor thermal environment in summer: an application, Build. Serv. Eng. Res. T. 34(3) (2012) 317-331. https://doi.org/10.1177/0143624412442512.

[23] J.-M. Seo, D. Song, K.H. Lee, Possibility of coupling outdoor air cooling and radiant floor cooling under hot and humid climate conditions, Energ. Buildings 81 (2014) 219-226. https://doi.org/10.1016/j.enbuild.2014.06.023.

[24] K.E. Gungor, R.H.S. Winterton, A general correlation for flow boiling in tubes and annuli, Int. J. Heat Mass Tran. 29 (1986) 351-358. https://doi.org/10.1016/0017-9310(86)90205-X.

[25] C. Yao, H. Li, Y. Xue, X. Liu, C. Hao, Investigation on the frictional pressure drop of gas liquid two-phase flows in vertical downward tubes, Int. Commun. Heat Mass 91 (2018) 138-149. https://doi.org/10.1016/j.icheatmasstransfer.201.

[26] D. Chisholm, A theoretical basis for the Lockhart-Martinelli correlation for two-phase flow, Int. J. Heat Mass Tran. 10 (1967) 1767-1778. https://doi.org/10.1016/0017-9310(67)90047-6.

[27] M.F. Modest, Radiative heat transfer, third ed., Elsevier Ltd, San Diego, 2013.

[28] L. Su, N. Li, X. Zhang, Y. Sun, J. Qian, Heat transfer and cooling characteristics of concrete

ceiling radiant cooling panel, Appl. Therm. Eng. 84 (2015) 170-179. https://doi.org/10.1016/j.applthermaleng.2015.0.

[29] H. Zhang, L. Jiang, W. Zheng, S. You, T. Jiang, S. Shao, X. Zhu, Experimental study on a novel thermal storage refrigerant-heated radiator coupled with air source heat pump heating system, Build. Environ. 164 (2019) 106341. https://doi.org/10.1016/j.buildenv.2019.106341.

[30] ISO, ISO 7730: Ergonomics of the Thermal Environment-Analytical Determination and Interpretation of Thermal Comfort Using Calculation of the PMV and PPD Indices and Local Thermal Comfort Criteria, International Organization for Standardization, Geneva, Switzerland, 2005.

[31] S. Bureerat, S. Srisomporn, Optimum plate-fin heat sinks by using a multi-objective evolutionary algorithm, Eng. Optimiz. 42 (2010) 305-323. https://doi.org/10.1080/03052150903143935.

[32] S. Yang, D. Zhou, Y. Wang, P. Li, Comparing impact of multi-factor planning layouts in residential areas on summer thermal comfort based on orthogonal design of experiments (ODOE), Build. Environ. 182 (2020). https://doi.org/10.1016/j.buildenv.2020.107145.

[33] H.B. Wang, Thermal performance test and analysis of a tube type radiation and convection air-conditioning device, Dalian University of Technology, 2014 (in Chinese).

[34] J.C. Chen, A correlation for boiling heat transfer to saturated fluids in convective flow, Ind. Eng. Chem. Pro. Des. Dev. 5 (1966) 322-329. https://doi.org/10.1021/i260019a023.

[35] M.G. Cooper, Saturation nucleate pool boiling - a simple correlation, National Conference on Heat Transfer, United Kingdom, 1984.

Credit Author Statement:

Tingting Jiang: Conceptualization, Methodology, Validation, Writing - Original Draft

Shijun You: Conceptualization, Resources, Writing – Reviewing and Editing

Zhangxiang Wu: Software, Investigation, Writing - Original Draft

Huan Zhang: Conceptualization, Formal analysis, Writing – Reviewing and Editing

Yaran Wang: Methodology, Software, Writing – Review & Editing,

Shen Wei: Writing – Review & Editing

Highlights:

1) A novel refrigerant-direct radiant cooling system is proposed.
2) The temperature distribution of the RDRC terminal surface is homogenous.
3) The mathematical and economic models of this terminal are established.
4) The sequencing of impact factors and the optimal structure are obtained.

Declaration of interests

☒ The authors declare that they have no known competing financial interests or personal relationships that could have appeared to influence the work reported in this paper.

☐The authors declare the following financial interests/personal relationships which may be considered as potential competing interests: